



On the investigation of size effect in bcc α -iron under high strain rate and high temperature: Multiscale dislocations dynamics simulations

Pascale El Ters^a, Mutasem A. Shehadeh^{a,b,*}

^a Department of Mechanical Engineering, American University of Beirut, Beirut, Lebanon

^b Department of Mechanical Engineering, Alfaisal University, Riyadh, Saudi Arabia

ARTICLE INFO

Keywords:

Size effect
Micro-polycrystalline BCC grains
Dislocation dynamics simulations
Hall-petch effect
Orowan effect

ABSTRACT

Size effect for BCC α -iron is investigated for micro-polycrystalline grains. MDDP simulations were performed to mimic impenetrable grain boundaries at sizes ranging between 0.5 μm and 2 μm at an applied rate of 10^5 s^{-1} at 300 K, 600 K and 900 K temperatures. For the three deformation temperatures, the Hall-Petch effect and the Orowan effect are reproduced. A comprehensive study of the microstructure evolution shows that screw dislocations control the plastic deformation of the polycrystalline materials via the activation of cross-slip mechanisms. Hardening is seen at low sizes for all temperatures at low strain range due to the dislocations pile up inside the grains prior to cross-slip activation. Once cross-slip is thermally activated, self-multiplication of dislocations is detected resulting in strain softening indicating that Orowan fit represented better the size effect in micro-polycrystalline BCC α -iron.

1. Introduction

Seven decades ago, Hall and Petch (Hall, 1951; Petch, 1953) empirically established a linear relationship between the yield strength of low carbon steel and the reciprocal of the square root of its grain size according to the Hall-Petch (H-P) equation:

$$\sigma_y = \sigma_0 + K_{HP}d^{-1/2} \quad (1)$$

Where σ_y is the yield strength of the material, d is the grain size, K_{HP} is a material constant (Cordero et al., 2016) and σ_0 is considered as the yield strength of a single bulk crystal (Cordero et al., 2016; Armstrong et al., 1962). Further studies showed that the H-P equation was applicable to several metals and alloys (Armstrong et al., 1962; Armstrong, 2014; Jago and Hansen, 1986) at submicron and micron range sizes.

Several models were proposed to explain the H-P equation. The first model was the pile up model explained first by Hall (1951) and elaborated by Eshelby (Eshelby et al., 1951), Hirth (Hirth and Lothe, 1982) and Chou et al. (Chou and Li, 1970). In this model, dislocations were assumed to pile up within the grains forming a stress concentration at the head of a slip band (Cordero et al., 2016; Armstrong, 2014; Naik and Walley, 2020). This model was refuted by Li (1963) where Hall-Petch effect was not attributed to the dislocation pile up but to the grain boundary (GB) source mechanism. The model of Li (1963) was further

developed by Ashby (1970). Ashby (1970) proposed a strain hardening model to derive the H-P equation. At yielding, GB ledges generate dislocations proportional to the grain size such that:

$$\rho_{GN} = \frac{\epsilon}{4db} \quad (2)$$

where ρ_{GN} is the geometrically necessary dislocation and ϵ is the strain. Alternatively, the increase of dislocation density affects the flow stress through Taylor's equation:

$$\sigma = \sigma_0 + \alpha Gb\sqrt{\rho} \quad (3)$$

Where σ_0 and α are material constants, G is the shear modulus, b is the Burgers vector and ρ is the dislocation density. Combining equations (2) and (3) leads to an inverse relationship between the flow stress and the square root of grain size.

Recently, the above two models were on an ongoing debate. From the source mechanism model, several work hardening models were suggested to explain the size effect (Naik and Walley, 2020). Cordero et al. (2016) summarized the various grain strengthening models over six decades and found that the strain hardening model of Ashby (1970) describes best the H-P equation. However, Li et al. (2016) argued these findings by conducting a Bayesian meta-analysis using the experimental data in the literature. They found that the data does not fit Ashby model.

* Corresponding author. Department of Mechanical Engineering, American University of Beirut, Beirut, Lebanon.

E-mail address: ms144@aub.edu.lb (M.A. Shehadeh).

Table 1

Sizes of the cubic grains used in the simulation with their initial dislocation density.

Grain Size (μm)	Initial dislocation density (m^{-2})	Number of Frank Read Sources
$0.2 \times 0.2 \times 0.2$	1.09×10^{13}	3
$0.75 \times 0.75 \times 0.75$	4.95×10^{12}	3
$1 \times 1 \times 1$	3.15×10^{12}	4
$1.5 \times 1.5 \times 1.5$	2.65×10^{12}	7
$2 \times 2 \times 2$	1.57×10^{12}	7

Li et al. (2016) suggest that the dislocation curvature is responsible for the grain strengthening mechanism. Line tension which is inversely proportional to the length of the source (L) is responsible for the bow out of a Frank Read source. Therefore, the yield stress is proportional to $1/L$ or $1/d$.

Along with the strengthening mechanism that is trying to explain the physics behind the H–P effect, the validity of equation (1) was also under discussion. Even though the Hall–Petch equation was applicable to many metals, several studies (Cordero et al., 2016; Conrad, 1963; Christman, 1993) showed that the exponent $n = -0.5$ may differ from one material to another. Christman (1993) fitted experimentally data on grain size and found out that the size exponent varies between -0.9 and -0.5 for BCC metals. Cordero et al. (2016) compiled the existing data for several materials and found that for BCC α -iron, n is equal to -0.29 and K_{HP} is equal to $640 \text{ MPa } \mu\text{m}^{0.29}$. Based on the dislocation curvature model, Dunstan and Bushby (2014a) statistically showed that the yield strength is linearly proportional to d^{-1} or to $\ln d/d$. Chandran (2019) noticed that σ_0 and K_{HP} in α -iron vary from one study to another; although they should not since they are material constants. He gathered all the data in the literature on the yield strength over multiple length scale and proposed a phenomenological exponential function.

In addition to the experimental works that had been done to explore the mechanism behind the Hall–Petch effect, atomistic and discrete dislocation dynamics (DDD) simulations were employed to identify the strengthening mechanism. Molecular dynamics simulations (Wang et al., 2014; Zhang et al., 2019; Van Swygenhoven, 2002) were carried out to study the interaction between the GB and dislocations. On the other hand, various strengthening models were proposed by carrying out DDD simulations. Lefebvre et al. (2007) used 2.5D to identify the dislocation mechanism governing the H–P effect in Copper micropillars. They found that the Hall–Petch equation is applicable, however, the controlling mechanisms change with grain sizes. For larger grain sizes, pile up model dominates the deformation mechanism, while for the ultrafine grain sizes, the dislocation mean free path is the controlling mechanism. Biner & Morris (Biner and Morris, 2003) showed that size effect is determined by dislocation pile up across the boundaries. Ohashi et al. (2007) noticed that the shortening of dislocation sources is responsible for the size effect. Zhou and LeSar (Zhou and Lesar, 2012) observed that the length of the spiral sources controls the strengthening mechanism. El-Awady (El-awady, 2015) revealed the importance of the dislocation density in predicting the controlling mechanism of the size effect. Once the dislocation density which is size dependent reaches a critical value, the dominant strengthening mechanism changes from dislocation source to forest hardening source. Li et al. (2009), Zhang et al. (2021) and Jiang et al., 2019, 2020 studied the influence of GB orientations on the size effect as well as the mechanical properties of micropillars. They found that for penetrable and impenetrable GB, size effect is consistent. Hardening and hence flow stress, are affected by the orientation of the GB. Most dislocation dynamics simulations used impenetrable grain boundaries to study size effect; some DDD simulations were carried out to emphasize on the influence of the dislocations – grain boundary interaction on size effect. Fan et al. (2015) studied the hardening effect in polycrystalline Mg by modeling twin boundaries in DDD. Espinosa et al., 2005, 2006 assumed that the nucleation of

dislocations at the grain boundaries are responsible for the size effect in thin film. Yellakara & Wang (Yellakara and Wang, 2014) explained the H–P effect in polycrystalline copper by studying the effect initial dislocation density and grain shape. Lu et al. (2022) constructed a penetrable GB model to study the dependence of size effect on source length and grain size. They found that the yield stress of polycrystalline sample with impenetrable GB is twice higher than those with penetrable GB due to dislocation pile up. Furthermore, the Hall–Petch equation was not satisfied, rather the exponent was found to be between 0.91 and 0.98.

Various models were proposed to explain the Hall–Petch effect, but no adopted model has yet been achieved. Due to the debatable investigations reported in the literature, there are still several features related to the effect of high temperature/high strain rate on the size effect equation as well as the dynamic evolution of dislocations that need to be addressed. Even though temperature plays a major role in the deformation mechanism of BCC metals and to the authors' best knowledge, there are no studies on the effect of high temperature on the Hall–Petch equation in BCC α -iron. In this work, we carried out Multiscale Dislocation Dynamics Plasticity (MDDP) simulations to study the size effect on BCC α -iron polycrystal subjected to high temperature and high strain rate. We observed and interpreted the dynamic evolution of the dislocations microstructure to identify the controlling mechanism of plastic deformation and grain strengthening. The simulations were conducted to mimic BCC α -iron micro polycrystalline subjected to a compressive loading of 10^5 s^{-1} at 300 K, 600 K and 900 K deformation temperatures. The cubic grain size varies from $0.5 \mu\text{m}$ to $2 \mu\text{m}$. The MDDP approach is described in the following section. Simulation results are discussed and analyzed in Section 3.

2. Methodology

Multiscale Dislocation Dynamics Plasticity (MDDP) (Zbib, 2002; Zbib and Diaz de la Rubia, 2002) is a hybrid elasto-visco-plastic model that accounts for the time dependent plasticity through the explicit 3D evaluation of dislocation nucleation, generation and motion. MDDP is a simulation model that couples the three dimensional discrete dislocation dynamics (DDD) with the macro level scale where the mass, momentum and energy transport obey the basic laws of continuum mechanics using finite element (FE) analysis (Yasin et al., 2001; Kattoura and Shehadeh, 2014). A noteworthy feature of the model is the incorporation of strain rate and temperature dependent mobility law based on atomistic calculations as discussed in (El Ters and Shehadeh, 2019; Gurrutxaga-Lerma, 2016; Gurrutxaga-Lerma et al., 2017) such that:

$$d(T, v, \theta) = \frac{d_0}{1 - \left(\frac{v}{c_t}\right)^2} \times \frac{T}{T_{cr}} \quad (4)$$

Where T is the simulation temperature; v is the glide velocity and θ is the dislocation character that is the angle between the dislocation line sense and its burger vector. T_{cr} is the critical temperature of the material which is the temperature above which the mobility of screw dislocation equalizes that of an edge dislocation ($T_{cr} = 340 \text{ K}$ for α -Fe); d_0 is the dislocation drag at the reference temperature ($d_0 = 9.4 \times 10^{-5} \text{ Pa s}$ at 340 K (Urabe and Weertman, 1975)); c_t is the material transverse speed of sound. The values of c_t are tabulated in Table 2. The lattice friction (σ) integrated in MDDP is the one used in (El Ters and Shehadeh, 2019; Gurrutxaga-Lerma et al., 2017; El Ters and Shehadeh, 2020):

$$\sigma = \sigma^p \times \frac{T}{T_{cr}} \quad (5)$$

where σ^p is equal to 500 MPa, 200 MPa and 50 MPa for pure screw, mixed and pure edge dislocation respectively (El Ters and Shehadeh, 2019).

Previous MDDP simulations (El Ters and Shehadeh, 2019, 2020) investigated the mechanical response and microstructure evolution of

Table 2
Mechanical properties of α -iron at different temperatures (El Ters and Shehadeh, 2019; Gurrutxaga-Lerma et al., 2017).

	300 K	600 K	900 K
Burgers vector b (nm)	0.248	0.248	0.248
Density ρ (kg.m ⁻³)	7860	7767	7600
Shear Modulus G (GPa)	116	100	62.5
Poisson ratio ν	0.37	0.39	0.43
c_t (m/s)	3197.22	2986.74	2634.41

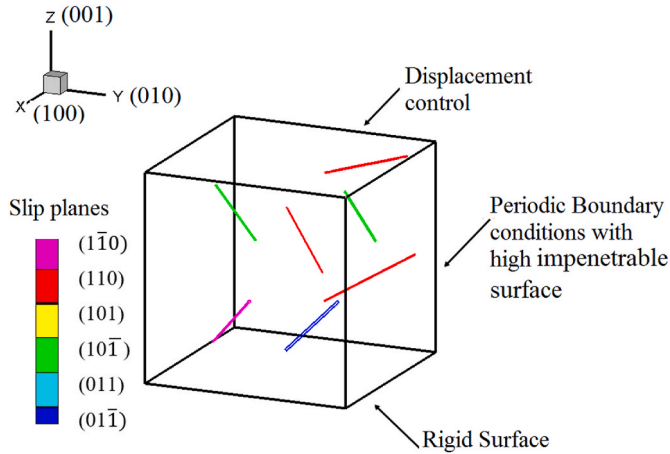


Fig. 1. MDDP simulation set up of the polycrystalline cubic α -iron. The colored straight pinned segments illustrate the Frank Read sources placed on the $\{110\}$ planes.

bulk BCC iron as well as BCC iron micropillars subjected to high strain rate and high temperature. Here we carried out MDDP simulations to mimic the mechanical response of micro-polycrystalline BCC iron. The micro-polycrystalline is simulated as an infinite periodic cluster made with one cubic grain. Cubic grains ranging from 0.5 μm to 2 μm (Table 1) are simulated to study the Hall-Petch effect (Fig. 1) where grains are oriented in the $[001]$ direction. In all these simulations, an initial dislocation density was taken between $2 \times 10^{12}\text{m}^{-2}$ and $1 \times 10^{13}\text{m}^{-2}$.

Frank Read (FR) sources were introduced randomly in the simulated domain to act as agents for dislocation generation and multiplication on the $\{110\}$ slip planes. The length of the dislocation sources is taken as one-third of the grain size (Zbib and Khraishi, 2008). To model impenetrable grain boundaries, we applied a large stress on the boundary of the grain such that the penetration of dislocations through boundaries is obstructed. The mechanical properties for the α -iron are listed in Table 2.

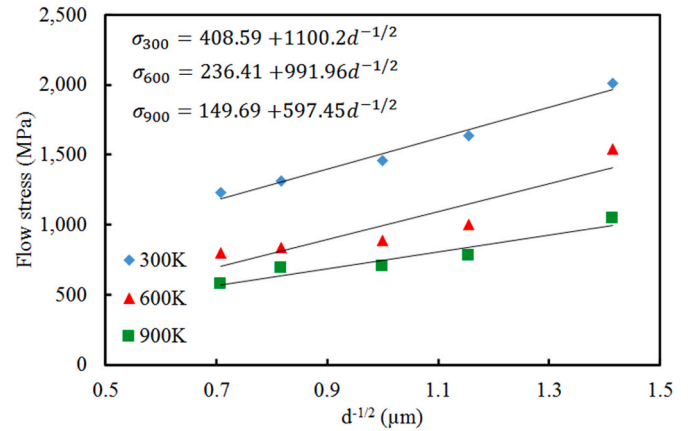


Fig. 3. Plot of the flow stress at 0.6% strain vs. $1/\sqrt{d}$ at 300 K, 600 K and 900 K.

Table 3
MDDP generated constant parameters of the Hall Petch equation at different temperatures as well as the correlation coefficient R^2 .

Temperature (K)	σ_0 (MPa)	Hall Petch constant K_{HP} (MPa. $\mu\text{m}^{1/2}$)	Correlation Coefficient R^2
300	408.59	1100.2	0.9775
600	236.41	991.96	0.8328
900	149.69	597.45	0.9079

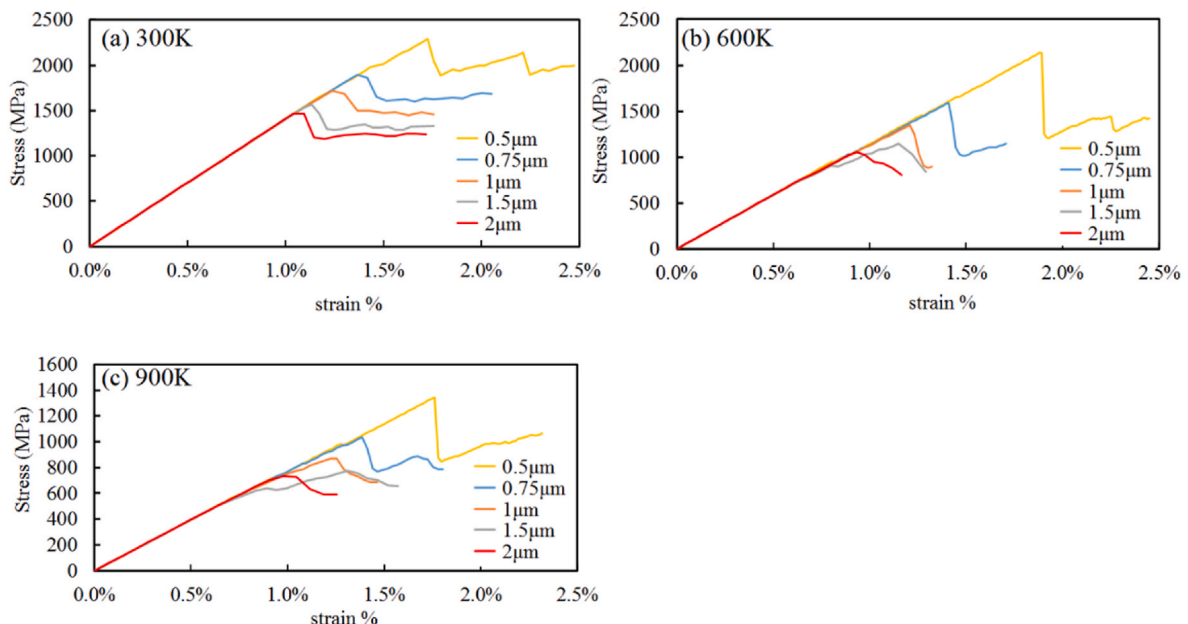


Fig. 2. Stress strain curves at different sizes for (a) 300 K, (b) 600 K and (c) 900 K.

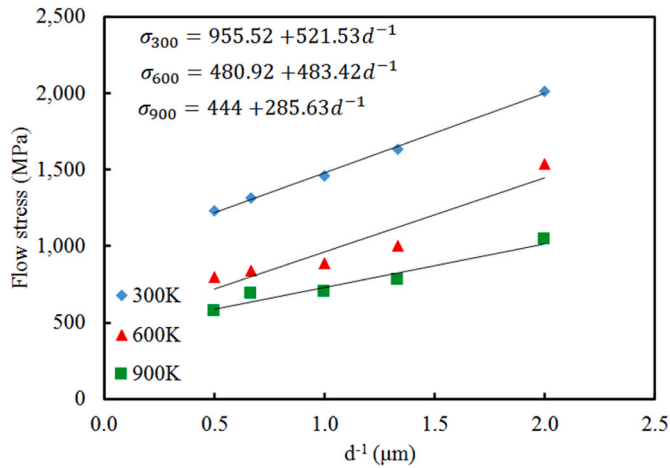


Fig. 4. Plot of the flow stress at 0.6% strain vs. $1/d$ at 300 K, 600 K and 900 K.

Table 4

Constant parameters of the Hall Petch equation at different temperatures according to Orowan equation as well as the correlation coefficient R^2 .

Temperature (K)	σ_0 (MPa)	K (MPa.μm)	Correlation Coefficient R^2
300	955.52	521.53	0.9972
600	480.92	483.42	0.8979
900	444	285.63	0.9422

3. Results and discussion

3.1. Size effect at $10^5 s^{-1}$

Fig. 2 shows the generated stress strain curves for the five simulated sizes subjected to a deformation rate of $10^5 s^{-1}$ and at different deformation temperatures (300 K, 600 K and 900 K). By inspecting Fig. 2(a), it is observed that for sizes greater than $0.75 \mu m$; the response is linearly elastic up to the onset of yielding followed by a stress drop to a constant flow stress value indicating stress relaxation. For the $0.5 \mu m$, three stages on the stress strain curves can be identified. First, the linear elastic regime followed by a linear plastic regime with different slope indicates apparent strain hardening at very low strain. This apparent strain hardening is followed by a serration behavior in the stress strain curve. This is attributed to the rapid increase of dislocation density followed by a decrease in the dislocation density evolution due to the storage of dislocations inside the confined grain. The serration characteristic in the $0.5 \mu m$ stress-strain curve indicates that there is a slight change in the deformation mechanism at smaller sizes as will be discussed shortly. The stress strain curves at 300 K are in good agreement with the results of (Okitsu et al., 2011; Tsuji et al., 2002) on α -iron. At higher temperatures, the stress strain behavior of the $0.5 \mu m$ at 300 K is also detected at $0.75 \mu m$. Furthermore, the amount of stress drop after reaching the peak is very large when compared to the stress drop at room temperature. The stress strain behavior at high temperature will be discussed in detail below.

Irrespective of the deformation temperature and strain values, it is clear from Fig. 2 that the flow stress decreases as the grain size increases. To quantify the size effect, the flow stress at 0.6% strain on the stress-

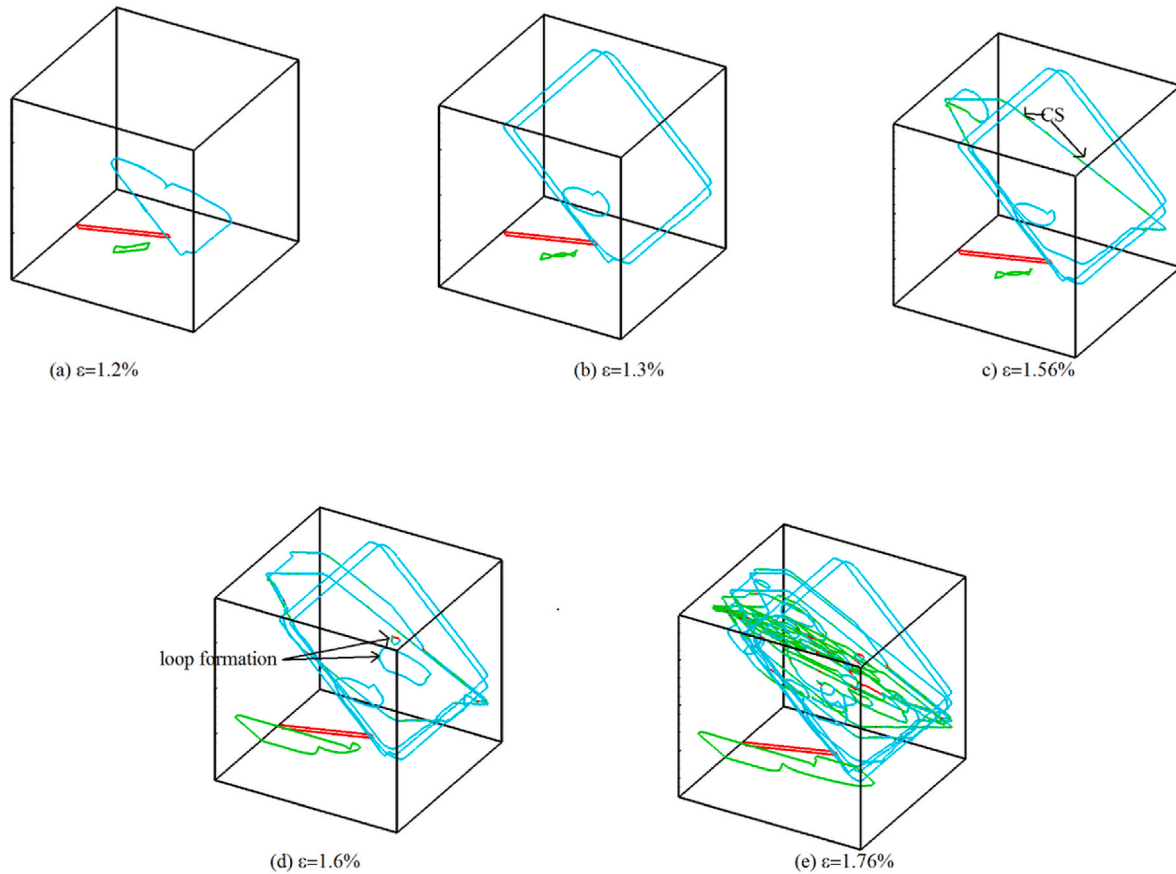


Fig. 5. Dislocation microstructure evolution of the $0.5 \mu m$ grain at room temperature and at different strain. (a) The Frank Read source lying on the (110) plane starts to bow out asymmetrically inside the grain. (b) Two dislocations pile up loops are formed inside the crystal at a strain of $\epsilon = 1.3\%$. (c) Cross-slip (CS) is activated at a strain of $\epsilon = 1.56\%$. (d) While the cross-slip mechanism is enhanced, additional loops are formed acting as obstacles to dislocation motion. (e) At a strain of 1.76% , dense network of dislocations is shown.

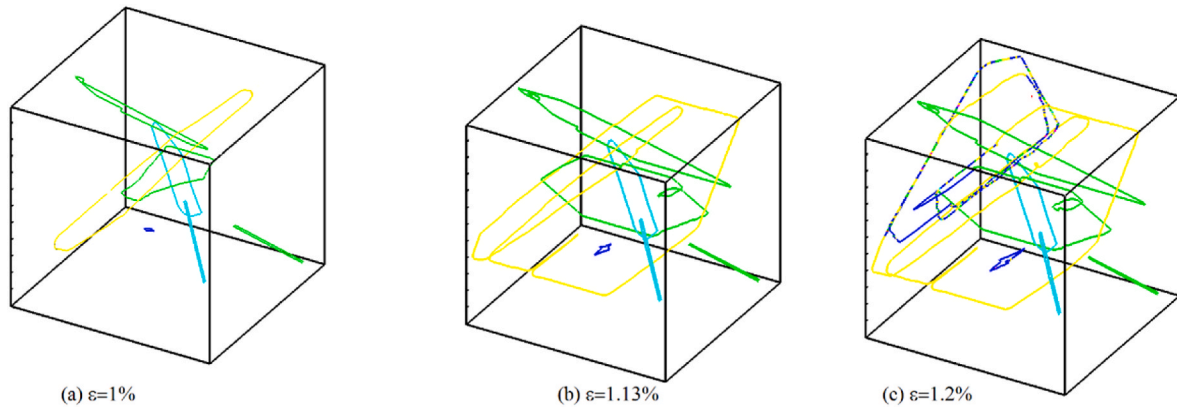


Fig. 6. Dislocation microstructure evolution of the 1.5 μm grain at room temperature and at different strain. (a) At a strain of 1%, Some Frank Read sources are activated while others are immobile. (b) Screw dislocations start to move at a strain of 1.13%. (c) Cross-slip mechanism is activated for the screw dislocation of the (101) plane.

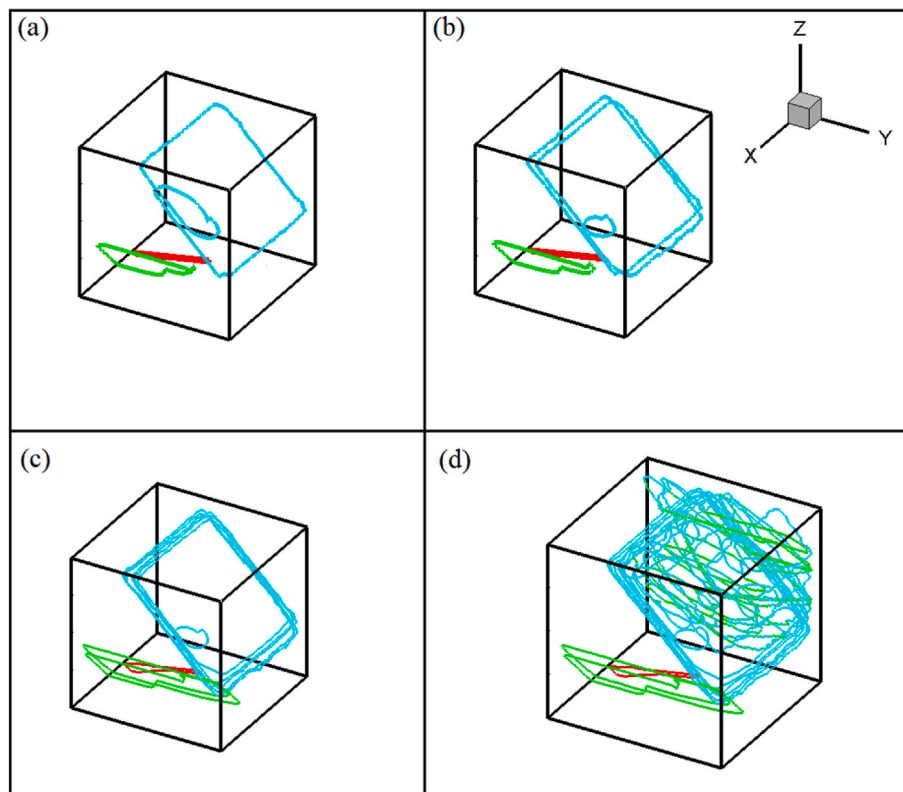


Fig. 7. Dislocation microstructure evolution of the 0.5 μm grain at 600 K and at different strain. (a) The (110) plane is activated with edge and screw dislocations moving at the same pace. (b) Dislocations pile up start to be seen. (c) More dislocations pile up are formed. (d) Cross-slip is activated resulting in an avalanche of dislocations.

strain curves for the three deformation temperatures is plotted vs. the reciprocal of the square root of the grain size in Fig. 3. As can be seen from Fig. 3, the stress vs. $d^{-1/2}$ relationship fits well the Hall-Petch equation (1) for the three deformation temperatures.

As can be seen from Fig. 3 and Table 3, K_{HP} as well as σ_0 are temperature dependent. In BCC metals, the flow stress is known to decrease with the deformation temperature (El Ters and Shehadeh, 2019; Reed-Hill et al., 2009) therefore σ_0 which is considered as the flow stress of a single α -iron crystal is expected to decrease as the deformation temperature increases. El Ters and Shehadeh (El Ters and Shehadeh, 2019) showed that for strain rates higher than or equal to $10^5 s^{-1}$, the effect of temperature on the flow stress is considerable with a power

dependency of -0.61 .

Like the dependency of σ_0 on temperature, Table 3 shows that the Hall-Petch constant K_{HP} decreases with the increasing deformation temperature. Armstrong et al. (Armstrong et al., 1962; Armstrong, 2014) proposed a model to evaluate the Hall-Petch constant such as:

$$K_{HP} = m \left[\pi \times m^* \times \frac{Gb\tau_{RSS}}{2\alpha} \right]^{1/2} \quad (6)$$

Where m is Taylor factor relating the compression strength to the resolved shear stress, m^* is a Sachs orientation factor, G is the shear modulus, b is the Burgers vector, τ_{RSS} the resolved shear stress required to induce the motion of dislocations across the grain boundary and α is a

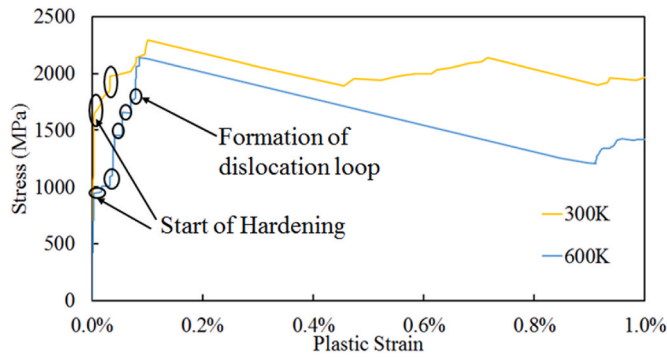


Fig. 8. Stress vs. plastic strain for the 0.5 μm at 300 K and 600 K.

material constant related to the Poisson ratio ν by $\frac{2(1-\nu)}{2-\nu}$. As can be seen from equation (6), the Hall-Petch constant is dependent on the shear modulus and the Poisson ratio of the material. However, G and ν are temperature dependent as depicted in Table 2, resulting in a temperature dependence of the Hall-Petch constant.

3.2. Size effect based on Orowan equation

To further investigate the stress dependency on size, we analyzed the dependency of the flow strength to the reciprocal of the grain size. Li et al. (2016) suggested that the dislocation curvature which is inversely proportional to the length of the source (L) is responsible for the grain strengthening mechanism. Therefore, the yield stress is related to the grain size by the following equation:

$$\sigma_f = \sigma_0 + Kd^{-1} \quad (7)$$

Where σ_f is the flow stress, d is the grain size, K is the Orowan strengthening constant and σ_0 is considered as the yield strength of a single bulk crystal. Fig. 4 shows that the flow stress fits well with the reciprocal of the grain size irrespective of temperature. Table 4 shows the values of σ_0 and K at the three deformation temperatures. By comparing Tables 3 and 4, it is evident that the MDDP generated σ_0 and K follow the same trend as the Hall-Petch constant with respect to temperature. It is interesting to note that even though the correlation coefficient R^2 for both the Orowan and Hall-Petch regression is high at all temperatures as shown in Tables 3 and 4, the value of the generated σ_0 for the Orowan equation is in good agreement with the MDDP generated flow stress of a single crystal (El Ters and Shehadeh, 2019) at the applied high deformation rate ($10^5 s^{-1}$). Therefore, one can conclude that the Orowan fit represents better the size effect than the Hall-Petch effect. This will be elaborated and explained in the microstructure evolution section (Section 3.3).

3.3. Microstructure and dislocation density evolution

As shown in Fig. 2, the change in the stress strain response at different sizes and different temperatures is due to the influence of the dislocations' velocity, mobility and lattice friction temperature dependence (El Ters and Shehadeh, 2019) (equation (4) and (5)). These parameters as well as the restricted space of the grains will affect dislocations activities and interactions. To shed light on the stress strain response and size effect presented in Section 3.1, microstructural analyses have been conducted on the 0.5 μm and 1.5 μm grains at 300 K and 600 K. Fig. 5 illustrates snap shots of the dislocation microstructure of the 0.5 μm at 300 K. Initially, the grain has three immobile Frank Read sources. The Frank Read source lying on the (011) slip plane starts to bow out asymmetrically indicating that its critical resolved shear stress is attained while the (110) and (10 $\bar{1}$) planes are not activated. The (10 $\bar{1}$) plane has zero Schmid factor while the critical resolved shear stress for the (110) plane is not attained yet. Due to high lattice friction imposed on the screw dislocations as shown in equation (5); edge dislocations start to move at low shear stress while screw dislocations remain idle (Fig. 5(a)), forming extended segments proportional to the grain size. As the edge dislocations continue to move inside the crystal, they are obstructed at the grain boundaries due to the extremely high stress imposed on the boundaries; thus, forcing them to form the first dislocation loop. As the loading increases, a second dislocation loop is formed at a strain of 1.3% (Fig. 5(b)). At this instant; the stress at the tip increases by 2τ due to the pile up model explained first by Hall (1951) and elaborated by Eshelby (Eshelby et al., 1951), Hirth (Hirth and Lothe, 1982) and Chou et al. (Chou and Li, 1970). In this model; the calculated stress at the head of the pile up τ_c is equal to the applied stress τ multiplied by the number of pile up (n). Consequently, hardening effect is observed in Fig. 2(a). At this strain, the lattice friction of screw dislocations is attained, and they start to glide slowly on their slip plane as compared to their edge counterparts. At a strain of 1.56%, stresses are high enough to thermally activate the cross-slip mechanism and screw dislocations cross-slip on the (10 $\bar{1}$) plane as depicted in Fig. 5(c). This resulted in the formation of small loops acting as obstacles (Fig. 5(d)) manifested in an increase of the stress in the stress-strain diagram (Fig. 2(a)). Fig. 5(d) also shows that the Frank Read source lying on the (10 $\bar{1}$) slip plane starts to bow out indicating that its critical resolved shear stress is exceeded by the applied stress at 1.6% strain. Additional screw dislocations are formed enhancing the cross-slip and double cross-slip processes and leading to an avalanche of dislocations throughout the simulation volume (Fig. 5(e)). The large interaction of dislocations inside the grain via self-multiplication is presented by an abrupt stress drop in the stress strain curve of Fig. 2(a). The cross-slip process of screw dislocations on the (10 $\bar{1}$) and (110) slip planes which have low and zero Schmid factor respectively along with the limited grain volume affected the mobility of dislocations resulting in an absence of dislocation generation. This is exhibited in the elastic loading between the strain jumps of the stress strain curve of Fig. 2(a). As the stress is increased, the cross-slip process of the (10 $\bar{1}$) plane is activated leading to a motion of

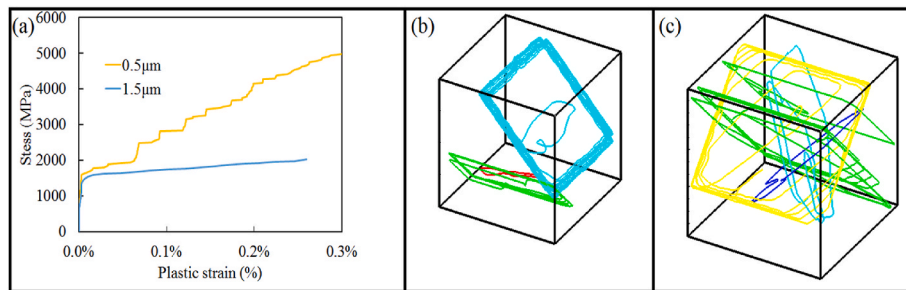


Fig. 9. (a) Plot of the stress vs plastic strain at 0.5 μm and 1.5 μm at 300 K. Strain hardening is clear for both sizes. (b) Microstructure evolution of dislocations with no cross slip at 0.5 μm (c) Microstructure evolution of dislocations with no cross-slip at 1.5 μm.

screw dislocations and dislocation generation.

For larger grains and as illustrated in Fig. 6, at room temperature, Frank Read sources are activated and edge dislocations start to move while screw dislocations are sessile. Once edge dislocations approach the boundaries, their motion is hindered leaving long sessile screw dislocations behind (Fig. 6(a)). Since the extended screws are proportional to the grain size, longer extended screw dislocations in the 1.5 μm grain are observed as compared to the extended one in the 0.5 μm grain. As a result, and as the loading proceeds, the lattice friction of screw dislocations is attained before the formation of the first loop. Screw dislocations start to move on their slip plane but at a lower speed than their edge counterparts (Fig. 6(b)). The increase in stresses allow the thermal activation of the cross-slip mechanism at a strain of 1.2%. As depicted in Fig. 6(c), the screw dislocation of the (101) plane exhibits a series of cross-slip and double cross-slip. Therefore, cross slip becomes dominant resulting in a large increase in dislocation density trapped in the simulation volume. It is worth noting that no dislocation pile up is observed for larger grains due to the earlier activation of cross-slip. The homogeneous deformation controlled by the self-multiplication of screw dislocations lead to the formation of a dense network of dislocations resulting in stress relaxation in the stress strain curve of Fig. 2(a). Since no dislocations pile up is shown due to the self-multiplication of dislocations, one can conclude that size effect is exhibited due to the dislocation curvature. However, Frank Read sources length is related to the grain size in MDDP as $L = d/3$ where L is the Frank Read source length. The generated MDDP results agree well with previous experimental and simulation results and analysis (Li et al., 2016; Dunstan and Bushby, 2013, 2014b).

To investigate the effect of temperature on size effect, snap shots of the 0.5 μm grains at 600 K are presented in Fig. 7. Once the critical resolved shear stress is attained, the Frank Read source placed on the (011) plane starts to bow out with screw and edge dislocations moving at the same time and at the same speed (equation (4) and (5)). As the strain increases (Fig. 7(b–c)), screw and edge dislocations advance towards the boundaries but cannot leave the grain. Dislocation loops are generated on their slip system and accumulated at the vicinity of the grain boundaries. The internal stresses emerged from the dislocation's accumulation exceeded the resolved shear stress of the (10 $\bar{1}$) slip plane. It is interesting to note that the dislocations lying on the (10 $\bar{1}$) start to pile up forming many loops as shown in Fig. 7(c). The number of accumulated loops at 0.5 μm is higher for the annealed grains than that for the room temperature ones. This is associated to the occurrence of the cross-slip and the motion of screw dislocations. The lattice friction of screw dislocations at higher temperature is smaller than the one at 300 K therefore screw dislocations at 600 K move faster and reaches the boundary at relatively low stresses. The accumulation of the loops makes them harder to be activated thus increasing the stress level which becomes high enough to thermally activate the cross-slip mechanism. Screw dislocations start to cross-slip and double cross-slip at high-speed compared to screws at room temperature; resulting in a rapid self-multiplication and a complex network of entangled dislocations is formed. The fast increase in dislocation generation resulted in a large stress drop as indicated in Fig. 2(b). Fig. 8 shows the plot of the stress vs. the plastic strain for the 0.5 μm at 300 K and 600 K deformation temperatures. From Fig. 8, each step corresponds to the formation of one dislocation loop. The hardening region at 600 K is greater than the 300 K one due to the mobility of screw dislocations. At 600 K, screw dislocations move faster than the 300 K thus requiring less external stress to be activated and consequently lower yield strength.

To elucidate the importance of cross-slip in the deformation mechanism of polycrystalline α -iron; we carried out MDDP simulations of the 0.5 μm and 1.5 μm grains at 300 K by disallowing the activation of cross-slip. Fig. 9 depicts the stress strain response of the 0.5 μm and 1.5 μm grains as well as their microstructure evolution. It can be seen from Fig. 9(a) that the flow stress continues to increase as the strain increases

leading to a significantly high strain hardening rate. Hardening is dominating the plastic flow. This can be attributed to the accumulation of dislocation loops near the boundaries (Fig. 9(b–c)). The impenetrable grain boundary impedes dislocations motion especially screw ones that are unable to cross-slip. The lack of mobility in the dislocations induces an increase in the flow stress and consequently hardening effect is presented.

4. Conclusion

In this study, MDDP simulations were carried out to investigate the Hall-Petch equation for polycrystalline BCC α -iron subjected to high strain rate at high deformation temperatures. For the three deformation temperatures and at different strain rates, our results are in line with the H–P fit and Orowan fit. However, the constant value of σ_0 in the size effect equation which is the flow stress of a bulk crystal is closer to the Orowan fit than the H–P fit. For all temperatures and at different sizes, the plastic deformation is controlled by screw dislocations resulting in a large self-multiplication of dislocations via cross-slip. For the 0.5 μm grain, there is a minor transition in the deformation mechanism where hardening is seen at low strain followed by strain softening. The hardening is the result of the dislocation pile up at the boundaries. At low temperature, sessile extended screws are formed as the Frank Read source is activated. These screws are proportional to the length size leading to a pile up before the thermal stress is reached to activate cross-slip mechanism. Once cross-slip is activated, strain softening is manifested. For greater sizes, no dislocations pile up loops are shown in the microstructure indicating that dislocation curvature controls plasticity instead of dislocations pile up. This led to the conclusion that the exponent $n = -1$ is a better fit for the size effect.

Author agreement statement

We the undersigned declare that this manuscript is original, has not been published before and is not currently being considered for publication elsewhere.

We confirm that the manuscript has been read and approved by all named authors and that there are no other persons who satisfied the criteria for authorship but are not listed. We further confirm that the order of authors listed in the manuscript has been approved by all of us.

We understand that the Corresponding Author is the sole contact for the Editorial process. He/she is responsible for communicating with the other authors about progress, submissions of revisions and final approval of proofs.

Declaration of competing interest

The authors declare that they have no known competing financial interests or personal relationships that could have appeared to influence the work reported in this paper.

Data availability

Data will be made available on request.

Acknowledgements

Support from the Research Board at the American University of Beirut is greatly acknowledged.

References

- Armstrong, R.W., 2014. 60 years of hall-petch: past to present nano-scale connections. *Mater. Trans.* 55, 2–12. <https://doi.org/10.2320/matertrans.MA201302>.
- Armstrong, R., Codd, I., Douthwaite, R.M., Petch, N.J., 1962. The plastic deformation of polycrystalline aggregates. *Philos. Mag.* 7, 45–58. <https://doi.org/10.1080/14786436208201857>.

- Ashby, M.F., 1970. The deformation of plastically non-homogeneous materials. *Philos. Mag.* 21, 399–424. <https://doi.org/10.1080/14786437008238426>.
- Biner, S.B., Morris, J.R., 2003. The effects of grain size and dislocation source density on the strengthening behaviour of polycrystals: a two-dimensional discrete dislocation simulation. *Philos. Mag.* 83, 3677–3690. <https://doi.org/10.1080/14786430310001599414>.
- Chandran, K.S.R., 2019. A new exponential function to represent the effect of grain size on the strength of pure iron over multiple length scales. *J. Mater. Res.* 34, 2315–2324. <https://doi.org/10.1557/jmr.2019.111>.
- Chou, Y.T., Li, J.C.M., 1970. The role of dislocations in the flow stress grain size relationships. *Metall. Mater. Trans. B* 1, 1145.
- Christman, T., 1993. Grain boundary strengthening exponent in conventional and ultrafine microstructure. *Scripta Metall. Mater.* [https://doi.org/10.1016/0956-716X\(93\)90581-C](https://doi.org/10.1016/0956-716X(93)90581-C).
- Conrad, H., 1963. Effect of grain size on the lower yield and flow stress of iron and steel. *Acta Metall.* 11, 75–77.
- Cordero, Z.C., Knight, B.E., Schuh, C.A., 2016. Six decades of the Hall–Petch effect – a survey of grain-size strengthening studies on pure metals. *Int. Mater. Rev.* 61, 495–512. <https://doi.org/10.1080/09506608.2016.1191808>.
- Dunstan, D.J., Bushby, A.J., 2013. The scaling exponent in the size effect of small scale plastic deformation. *Int. J. Plast.* 40, 152–162. <https://doi.org/10.1016/j.ijplas.2012.08.002>.
- Dunstan, D.J., Bushby, A.J., 2014a. Grain size dependence of the strength of metals: the Hall–Petch effect does not scale as the inverse square root of grain size. *Int. J. Plast.* 53, 56–65. <https://doi.org/10.1016/j.ijplas.2013.07.004>.
- Dunstan, D.J., Bushby, A.J., 2014b. Grain size dependence of the strength of metals: the Hall – Petch effect does not scale as the inverse square root of grain size. *Int. J. Plast.* 53, 56–65. <https://doi.org/10.1016/j.ijplas.2013.07.004>.
- El-awady, J.A., 2015. dislocation-mediated plasticity. *Nat. Commun.* 6, 1–9. <https://doi.org/10.1038/ncomms6926>.
- Eshelby, J.D., Frank, F.C., Nabarro, F.R.N., 1951. XLI. The equilibrium of linear arrays of dislocations. *London, Edinburgh, Dublin Philos. Mag. J. Sci.* 42, 351–364. <https://doi.org/10.1080/14786445108561060>.
- Espinosa, H.D., Berbenni, S., Panico, M., Schwarz, K.W., 2005. An interpretation of size-scale plasticity in geometrically confined systems. *Proc. Natl. Acad. Sci. U.S.A.* 102, 16933–16938. <https://doi.org/10.1073/pnas.0508572102>.
- Espinosa, H.D., Panico, M., Berbenni, S., Schwarz, K.W., 2006. Discrete dislocation dynamics simulations to interpret plasticity size and surface effects in freestanding FCC thin films. *Int. J. Plast.* 22, 2091–2117. <https://doi.org/10.1016/j.ijplas.2006.01.007>.
- Fan, H., Aubry, S., Arsenlis, A., El-awady, J.A., 2015. The role of twinning deformation on the hardening response of polycrystalline magnesium from discrete dislocation dynamics simulations. *Acta Mater.* 92, 126–139. <https://doi.org/10.1016/j.actamat.2015.03.039>.
- Gurrutxaga-Lerma, B., 2016. The role of the mobility law of dislocations in the plastic response of shock loaded pure metals. *Model. Simulat. Mater. Sci. Eng.* 24, 065006. <https://doi.org/10.1088/0965-0393/24/6/065006>.
- Gurrutxaga-Lerma, B., Shehadeh, M.A., Balint, D.S., Dini, D., Chen, L., Eakins, D.E., 2017. The effect of temperature on the elastic precursor decay in shock loaded FCC aluminium and BCC iron. *Int. J. Plast.* 96, 135–155. <https://doi.org/10.1016/j.ijplas.2017.05.001>.
- Hall, E.O., 1951. The deformation and ageing of mild steel: III discussion of results. *Proc. Phys. Soc. B* 64, 747–753. <https://doi.org/10.1088/0370-1301/64/9/303>.
- Hirth, J.P., Lothe, J., 1982. *Theory of Dislocations*. Krieger Publishing Company. <https://books.google.com.lb/books?id=LFZGAAAAAJ>.
- Jago, R.A., Hansen, N., 1986. Grain size effects in the deformation of polycrystalline iron. *Acta Metall.* 34, 1711–1720. [https://doi.org/10.1016/0001-6160\(86\)90118-5](https://doi.org/10.1016/0001-6160(86)90118-5).
- Jiang, M., Devincere, B., Monnet, G., 2019. Effects of the grain size and shape on the flow stress: a dislocation dynamics study. *Int. J. Plast.* 113, 111–124. <https://doi.org/10.1016/j.ijplas.2018.09.008>.
- Jiang, M., Monnet, G., Devincere, B., 2020. On the origin of the Hall–Petch law: a 3D-dislocation dynamics simulation investigation. *SSRN Electron. J.* <https://doi.org/10.2139/ssrn.3681164>.
- Kattoura, M., Shehadeh, M.A., 2014. On the ultra-high-strain rate shock deformation in copper single crystals: multiscale dislocation dynamics simulations. *Phil. Mag. Lett.* 94, 415–423. <https://doi.org/10.1080/09500839.2014.920540>.
- Lefebvre, S., Devincere, B., Hoc, T., 2007. Yield stress strengthening in ultrafine-grained metals: a two-dimensional simulation of dislocation dynamics. *J. Mech. Phys. Solid.* 55, 788–802. <https://doi.org/10.1016/j.jmps.2006.10.002>.
- Li, J.C.M., 1963. Petch relation and grain boundary sources. *Trans. Metall. Soc. AIME.* 227, 239.
- Li, Z., Hou, C., Huang, M., Ouyang, C., 2009. Strengthening mechanism in micro-polycrystals with penetrable grain boundaries by discrete dislocation dynamics simulation and Hall – Petch effect. *Comput. Mater. Sci.* 46, 1124–1134. <https://doi.org/10.1016/j.commatsci.2009.05.021>.
- Li, Y., Bushby, A.J., Dunstan, D.J., 2016. The Hall–Petch effect as a manifestation of the general size effect. *Proc. R. Soc. A Math. Phys. Eng. Sci.* 472 <https://doi.org/10.1098/rspa.2015.0890>.
- Lu, S., Kan, Q., Zaiser, M., Li, Z., Kang, G., Zhang, X., 2022. Size-dependent yield stress in ultrafine-grained polycrystals: a multiscale discrete dislocation dynamics study. *Int. J. Plast.* 149, 103183 <https://doi.org/10.1016/j.ijplas.2021.103183>.
- Naik, S.N., Walley, S.M., 2020. The Hall–Petch and inverse Hall–Petch relations and the hardness of nanocrystalline metals. *J. Mater. Sci.* 55, 2661–2681. <https://doi.org/10.1007/s10853-019-04160-w>.
- Ohashi, T., Kawamukai, M., Zbib, H., 2007. A multiscale approach for modeling scale-dependent yield stress in polycrystalline metals. *Int. J. Plast.* 23, 897–914. <https://doi.org/10.1016/j.ijplas.2006.10.002>.
- Okitsu, Y., Takata, N., Tsuji, N., 2011. Dynamic deformation behavior of ultrafine-grained iron produced by ultrahigh strain deformation and annealing. *Scripta Mater.* 64, 896–899. <https://doi.org/10.1016/j.scriptamat.2011.01.026>.
- Petch, N.J., 1953. The cleavage strength of polycrystals. *J. Iron Steel Institute* 174.
- Reed-Hill, R.E., Abbaschian, R., Abbaschian, L., 2009. *Physical Metallurgy Principles. fourth, Cengage Learning, Stamford, CT.*
- Van Swygenhoven, H., 2002. Grain boundaries and dislocations. *Science (80-)* 296, 66–68. <https://doi.org/10.1126/science.1071040>.
- El Ters, P., Shehadeh, M.A., 2019. Modeling the temperature and high strain rate sensitivity in BCC iron: atomistically informed multiscale dislocation dynamics simulations. *Int. J. Plast.* 112, 257–277. <https://doi.org/10.1016/j.ijplas.2018.09.002>.
- El Ters, P., Shehadeh, M.A., 2020. On the strain rate sensitivity of size-dependent plasticity in BCC iron at elevated temperatures : discrete dislocation dynamics investigation. *Mech. Mater.* 148, 103494 <https://doi.org/10.1016/j.mechmat.2020.103494>.
- Tsuji, N., Ito, Y., Saito, Y., Minamino, Y., 2002. Strength and ductility of ultrafine grained aluminum and iron produced by ARB and annealing. *Scripta Mater.* 47, 893–899. [https://doi.org/10.1016/S1359-6462\(02\)00282-8](https://doi.org/10.1016/S1359-6462(02)00282-8).
- Urabe, N., Weertman, J., 1975. Dislocation mobility in potassium and iron single crystals. *Mater. Sci. Eng.* 18, 41–49. [https://doi.org/10.1016/0025-5416\(75\)90071-3](https://doi.org/10.1016/0025-5416(75)90071-3).
- Wang, J., Beyerlein, I.J., Tomé, C.N., 2014. Reactions of lattice dislocations with grain boundaries in Mg: implications on the micro scale from atomic-scale calculations. *Int. J. Plast.* 56, 156–172. <https://doi.org/10.1016/j.ijplas.2013.11.009>.
- Yasin, H., Zbib, H.M., Khaleel, M.A., 2001. Size and boundary effects in discrete dislocation dynamics : coupling with continuum finite element. *Mater. Sci. Eng.* 309–310, 294–299.
- Yellakara, R.N., Wang, Z., 2014. A three-dimensional dislocation dynamics study of the effects of grain size and shape on strengthening behavior of fcc Cu. *Comput. Mater. Sci.* 87, 253–259. <https://doi.org/10.1016/j.commatsci.2014.02.037>.
- Zbib, H.M., 2002. *Multiscale Dislocation Dynamics Plasticity*.
- Zbib, H.M., Diaz de la Rubia, T., 2002. A multiscale model of plasticity. *Int. J. Plast.* 18, 1133–1163. [https://doi.org/10.1016/S0749-6419\(01\)00044-4](https://doi.org/10.1016/S0749-6419(01)00044-4).
- Zbib, H.M., Khraishi, T.A., 2008. Size Effects and Dislocation – Wave Interaction in Dislocation Dynamics. Elsevier Masson SAS. [https://doi.org/10.1016/S1572-4859\(07\)00004-6](https://doi.org/10.1016/S1572-4859(07)00004-6).
- Zhang, Z., Shao, C., Wang, S., Luo, X., Zheng, K., Urbassek, H.M., 2019. Interaction of dislocations and interfaces in crystalline heterostructures: a review of atomistic studies. *Crystals* 9. <https://doi.org/10.3390/cryst9110584>.
- Zhang, X., Lu, S., Zhang, B., Tian, X., Kan, Q., Kang, G., 2021. Dislocation–grain boundary interaction-based discrete dislocation dynamics modeling and its application to bicrystals with different misorientations. *Acta Mater.* 202, 88–98. <https://doi.org/10.1016/j.actamat.2020.10.052>.
- Zhou, C., Lesar, R., 2012. Dislocation dynamics simulations of plasticity in polycrystalline thin films. *Int. J. Plast.* 30–31, 185–201. <https://doi.org/10.1016/j.ijplas.2011.10.001>.